

A New Spectral Index for Mapping Water Surfaces in Urban Contexts

Eduardo Felix Justiniano ^a, Fernando Shinji Kawakubo ^a, Edimilson Rodrigues dos Santos Junior ^b,
Breno Malheiros de Melo ^c, Gustavo Paixão Menezes ^b, Marcel Fantin ^d, Julio Cesar Pedrassoli ^d,
Marcos Roberto Martines ^e, Rúbia Gomes Morato ^a

^a University of São Paulo – USP, Department of Geography, Brazil

^b University of São Paulo – USP, São Carlos School of Engineering, Brazil

^c Department of Urban Engineering, Federal University of São Carlos

^d University of São Paulo – USP, School of Architecture and Urbanism

^e School of Environment, Geography, and Sustainability (SEGS) - Western Michigan University

^e Federal University of São Carlos – UFScar, Department of Geography, Tourism and
Humanities, Brazil

Correspondence to: Eduardo Felix Justiniano (e.justiniano@alumni.usp.br)

**This manuscript is a non-peer-reviewed preprint submitted to EarthArXiv to ensure
rapid and free access to the work.**

A New Spectral Index for Mapping Water Surfaces in Urban Contexts

Eduardo Felix Justiniano ^a, Fernando Shinji Kawakubo ^a, Edimilson Rodrigues dos Santos Junior ^b, Breno Malheiros de Melo ^c, Gustavo Paixão Menezes ^b, Marcel Fantin ^d, Julio Cesar Pedrassoli ^d, Marcos Roberto Martines ^e, Rúbia Gomes Morato ^a

^a University of São Paulo – USP, Department of Geography, Brazil

^b University of São Paulo – USP, São Carlos School of Engineering, Brazil

^c Department of Urban Engineering, Federal University of São Carlos

^d University of São Paulo – USP, School of Architecture and Urbanism

^e School of Environment, Geography, and Sustainability (SEGS) - Western Michigan University

^e Federal University of São Carlos – UFScar, Department of Geography, Tourism and Humanities, Brazil

Abstract — This paper proposes a modification of MNDWI called Rescaled Water Index, aiming to enhance the delineation and performance of water body mapping in urban areas using satellite imagery. To evaluate the effectiveness of the proposed index, we compare its performance in mapping water surfaces in different cities in South America with the results obtained by other well-known water indices in the literature (namely, NDWI, MNDWI, AWEI_{sh}, and AWEI_{nsh}). We utilized images from the Sentinel satellites (2A and 2B), all acquired in June 2021, focusing on cities located south of the Tropic of Capricorn to obtain images with the highest incidence of shading, whose spectral response complicates the mapping of water surfaces without commission errors. In this scenario, the present study revealed that selecting the best single index for mapping all water surfaces is an arduous task, as their performances varied across the analyzed locations. Overall, the performance of the indices, evaluated by partial receiver operating characteristic curve and non-water misclassification point restrictions, revealed quite close but different results, especially considering the Rescaled Water Index, NDWI, and MNDWI. In the six areas analyzed, the Rescaled Water Index outperformed in three. Additionally, when considering the results for all the cities, the Rescaled Water Index outperformed in all the analyses. Such results, therefore, are interpreted as an essential contribution to water body mapping, considering its practical applications in environmental monitoring and water resource management in urbanized areas.

Keywords: Image classification, spectral analysis, urban area, water

I. INTRODUCTION

According to Shiklomanov and Rodda [1], about three-quarters of our planet is covered by water, of which 5% comprises the surfaces of rivers, lakes, and glaciers. Freshwater, including that found in subsurface sources, accounts for approximately 2.5% of the total volume of the hydrosphere [1]. Given its extensive coverage on the globe, water surfaces (WSs) play a vital role in the functioning

of the environment, directly and indirectly influencing climate mechanisms, the hydrological cycle, ecosystem interactions, and human activities [2], [3]. Thus, due to its significance with repercussions at different scales of approach, there is a growing demand to accurately quantify the temporal-spatial extents and variabilities of WSs through observations made by terrestrial resource satellites [4], [5], [6].

In the context of urban areas, mapping WSs serves numerous purposes, including supporting policies aimed at both water resource sustainability - such as water quality monitoring [7], [8], [9], and mitigating social and environmental impacts, such as floods caused by urban growth and climate change [10], [11]. To address these impacts, managers should focus on practices and actions that make cities more resilient [12], [13]. In addition to floods, WSs play a crucial role in mitigating temperature [14], [15], increasing air humidity levels [16], and influencing wind patterns [17] in their surroundings, serving as an essential local climate regulation ecosystem service [18]. On the other hand, WSs in urban areas also constitute significant sources of greenhouse gas emissions, contributing to global warming [19].

On a first approach, without delving into the environment's complexity, delineating WSs through remote sensing imagery seems to be easily achievable. This is because the spectral characteristics of water bodies themselves result in low reflectance of energy in the near-infrared (Nir) and shortwave infrared (Swir) channels [20], appearing as different tones in the image, which distinguishes them from emerging areas [21]. However, the water column is composed of mixtures of organic and inorganic materials, so depending on the concentration of these materials, the spectral signature of water bodies can vary drastically, making correct identification challenging [21]. For example, lakes can be classified according to the presence of nutrients, ranging from oligotrophic to eutrophic, which, in the presence of light, can favor the development of phytoplankton and possibly algae [22], [23], as well as the spectral response variation concerning the concentration of suspended materials [24], [25].

Another important consideration is that the composition and extent of WSs are highly variable in space and time [5], [26], [27]. These variations depend on factors such as terrain characteristics - including rock types, soil, and vegetation - and human activities - associated with agriculture and civil construction - which accelerate river systems' hydrodynamic and morphodynamic processes [28]. In addition to the conditions of the aquatic environment itself, mapping uncertainties can also stem from variations in solar illumination angles and sensor viewing angles [29], which can eventually interfere with confusion involving water and other classes with low-energy reflection, such as paved roads and building shadows [30], [31], [32].

One of the most used methods to map WSs is by generating index images, where different spectral bands are combined to enhance water bodies and increase their distinction from other land classes. A spectral index is generated through mathematical operations involving ratios, differences, normalization, multiplication, and others using physical values or digital numbers from two or more bands [33]. The first spectral index constructed for water, the Normalized Difference Water Index (NDWI), was proposed by McFeeters [34], who combined spectral bands from green visible light and Nir to enhance water while simultaneously eliminating the presence of soil and terrestrial vegetation. Subsequently, Xu [35] proposed a modification to NDWI by replacing the Nir band with the Swir1 band. This modified NDWI (MNDWI) is more suitable for enhancing and extracting water information in regions with a background dominated by built-up land areas because it reduces noise from built-up areas over NDWI. Since then, several other indices have been proposed in the literature and compared to assess their performance in different scenarios worldwide. Among them, we can mention the Automated Water Extraction Indexes (AWEI_{nsh} and AWEI_{sh}) [30], the Simple Water Index [36], the Multi-spectral Water Index [37], and the Automated Water Extraction Model in Complex Environment [38].

Despite the variety of spectral indices aimed at enhancing water bodies, there is still no consensus on the best index developed to date for mapping WSs. Some studies have proposed adopting strategies that combine different spectral indexes to improve the potential for water information extraction and reduce classification errors [32], [33], [39], [40]. Jiang et al. [39], for example, combined information extracted from vegetation indices such as NDVI [41], built-up area index NDBI [42], and MNDWI to delineate water surfaces through a transformation of the RGB-HSI color space. Subsequently, they created a second HSI image combining the blue and Nir bands and NDVI to remove shadows classified as water.

Therefore, given the numerous challenges still present in mapping WSs, this study proposes a new spectral index focused on water body mapping, considering the confusions commonly encountered, especially water, low energy reflecting urban materials, and other artifacts such as building shadows. Our index, the Rescaled Water Index (RWI), is compared with other existing water indices in the literature to demonstrate its effectiveness for different scenarios in South America.

II. II. METHOD

A. Satellite images

For the proposition and analysis of the RWI, we used multispectral images from the Sentinel 2A and 2B satellites with surface reflectance values (Table 1). Geographical cutouts containing WSs and tall buildings located in the cities of São Paulo, Curitiba, Florianópolis, Porto Alegre (Brazil), Buenos Aires (Argentina), and Viña del Mar (Chile) were selected. All cities are located south of the Tropic of Capricorn (-23.27°), which favors the occurrence of significant shadow presence in the images. We chose images without clouds acquired all in June (with azimuth and zenith angles ranging from 28.8 to 30.8 and from 53.2 to 64.1, respectively), the month of the winter solstice in the Southern Hemisphere when shadows from tall buildings are more pronounced. If more than one image was recorded in the month, we selected the image visually showing the highest tide level to achieve greater water surface detection.

TABLE 1: Images used in the study and acquisition parameters.

City/Country	Centroid of the selected areas	Sentinel-2 image	Mean solar angle	
			Azimuth	Zenithal
São Paulo (Brazil)	-46.67702, -23.58752	20210605T131249_20210605T131243_T23KLP	30.8	53.2
Curitiba (Brazil)	-49.29172, -25.43496	20210613T132231_20210613T132548_T22JFS	30.5	55.6
Florianópolis (Brazil)	-48.55586, -27.59260	20210613T132231_20210613T132548_T22JGQ	28.8	56.7
Porto Alegre (Brazil)	-51.22097, -30.03500	20210613T132231_20210613T132548_T22JDM	30.6	60.3
Buenos Aires (Argentina)	-58.44039, -34.55563	20210617T135119_20210617T135609_T21HUB	28.9	64.1
Viña del Mar (Chile)	-71.54578, -33.01574	20210607T143731_20210607T144845_T19HBD	29.7	62.0

B. Proposed index

To increase the separability between pixels corresponding to WSs and non-water surfaces (non-WSs) and thus improve the performance of systematic water body mapping, we propose a new index called RWI in this study. This proposition is an adaptation of the well-known MNDWI index [35], where we use the shortwave infrared 1 (Swir1) bands and insert an exponential scale, using Euler's number, in the green channel band and an adjustment factor n . The formulas are:

$$RWI = \frac{Green^{e^{-1}} \cdot n^{-1} - Swir1}{Green^{e^{-1}} \cdot n^{-1} + Swir1} \quad (1)$$

$$n = \frac{m_d(Green^{e^{-1}})}{m_d(Green)} \quad (2)$$

Where: $Green$ is the green band. $Swir1$ is the shortwave infrared 1 band. e is the Euler's number (~ 2.71828). m_d is the median value in the region of interest. $Green$ and $Swir1$ bands must be in surface reflectance values, not rescaled.

Modifying the green band using the Euler base root alters the median and increases the amplitude of the data. Dividing the values by the adjustment factor n allows the final dataset to exhibit a median value close to the original data and reduced variance (Fig. 1).

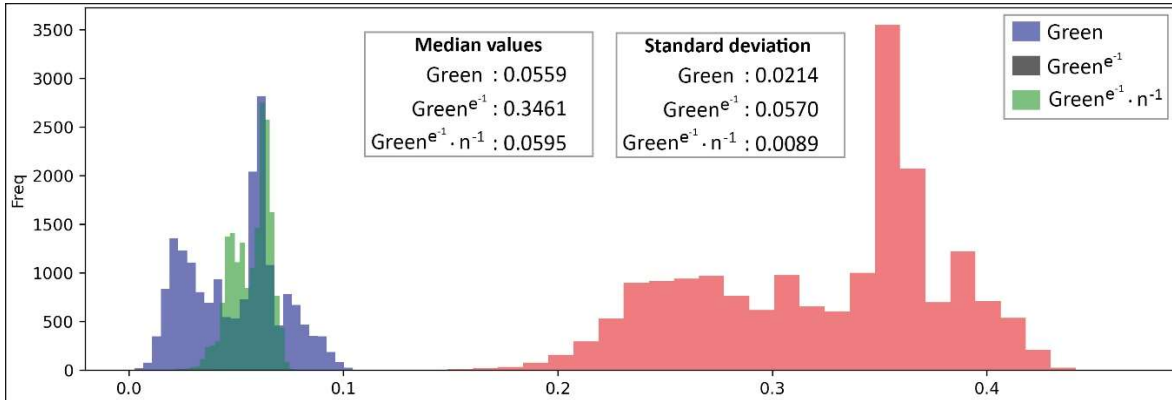


Fig. 1. Histograms of the $Green$ band and its modifications.

As multispectral images from Sentinel were used in the study, and the bands have variations in spatial resolution (between 10 and 60 m) according to different intervals of the electromagnetic spectrum, we adopted as reference the resolution recorded in the wavelength band of green, which has 10 m on the ground. Therefore, the $Swir1$ band, which has 20 m, was resampled to 10 m to match the pixel size of the two bands used to calculate the RWI.

Knaeps et al. [43], Uudeberg et al. [44], and Soomets et al. [22] have reported on the variability of reflectance in the green band in various water bodies. In our proposal, the exponential scale reduces the amplitude of the green band reflectance values, while the adjustment factor n^{-1} is employed to reduce the $Green^{e^{-1}}$ median value close to $Green$ median value.

C. Evaluation of the proposed index

1) Comparison with other spectral indices

As previously mentioned, the effectiveness of the RWI was checked by comparing its performance in discriminating WSs from non-WSs with the performances obtained with other well-known indexes in the literature (Table 2). Thus, we compared the effectiveness of RWI with the indices NDWI (3), MNDWI (4), $AWEI_{sh}$ (5), and $AWEI_{nsh}$ (6).

2) Reference samples

Reference samples were collected to support the performance analysis obtained with the various indices. Samples representing WSs and Non-WSs were carefully selected in a supervised manner based on the visual interpretation of the images (Table 1). High-resolution images from Google Earth were also used to aid in identifying different targets.

We selected 123,500 sample points, respecting the minimum spatial sample distance of one pixel to avoid spatial sample duplication at the same pixel. From this sampling universe, 18,000 points are located in WSs and 105,000 in Non-WSs. WS points are distributed across areas such as lagoons, treatment plants, rivers, and near the coastline or edges - in the case of seas, river mouths, and lakes. Non-WS points are distributed in areas with tall buildings casting shadows, as well as in regions with different types of vegetation, buildings, exposed soil, and sand strips on the ground, which may or may not be shaded (Fig. 2).

Fig. 3 illustrates the sample selection process and the possible hits and errors contained in the mapping, represented by True Positive (TP), True Negative (TN), False Positive (FP), and False Negative (FN).

TABLE 2: Indices used in the evaluation of WSs mapping.

Index	Author	Range
$RWI = \frac{Green^{e^{-1}} \cdot n^{-1} - Swir1}{Green^{e^{-1}} \cdot n^{-1} + Swir1} \quad (1)$	Our proposal	-1 to +1
$n = \frac{m_a(Green^{e^{-1}})}{m_a(Green)} \quad (2)$		
$NDWI = \frac{green - Nir}{green + Nir} \quad (3)$	McFeeters [34]	-1 to +1
$MNDWI = \frac{green - Swir1}{green + Swir1} \quad (4)$	Xu [35]	-1 to +1
$AWEI_{sh} = blue + 2.5 \cdot green - 1.5 \cdot (Nir + Swir1) - 0.25 \cdot Swir2 \quad (5)$	Feyisa et al. [30]	Indeterminate
$AWEI_{nsh} = 4 \cdot (green - Swir1) - (0.25 \cdot Nir + 2.75 \cdot Swir2) \quad (6)$		



Fig. 2. Distribution areas of water sample points (cyan) and urban areas with shadow occurrence (red).

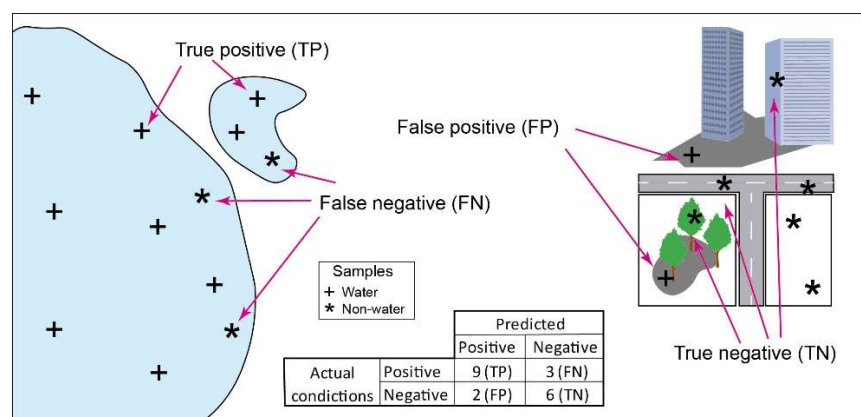


Fig. 3. The sampling scheme adopted in the study, with samples of Water Surfaces (WSs) and Non-Water Surfaces and the possible hits and errors (TP, TN, FP, and FN) that may be encountered in the mapping.

It is important to note that strips on the ground comprising the edges of water bodies were avoided in the sampling due to the seasonal variability of water level heights and the spectral mixture between

aquatic and non-aquatic elements, which could make the analysis more complicated. This is also one of the reasons why we chose to select Sentinel images acquired during higher tide periods. After this step, the values of the corresponding pixels of the RWI, NDWI, MNDWI, $AWEI_{sh}$, and $AWEI_{nsh}$ indices were extracted for each selected sample.

3) Data analysis

Considering the quantities of hits and errors obtained with the samples (Fig. 1), three statistical analyses were performed to check the efficiency of the indices in separating WSs and Non-WSs (Table 3). The first one considered the area under a segment of the Receiver Operating Characteristic curve (pROC), where the False Positive Rate (FPR) is less than or equal to 0.02, thus considering a maximum error of 2%, which allows for better observation of the curve's behavior near the TPR axis, in a range of high specificity. The comparison of pROC area values between the indices indicates the efficiency of one classifier, in relation to the other, in discriminating WSs in the considered slicing intervals.

In the second analysis, TPRmax was considered for $FPR = 0$, corresponding to the length of the ROC curve tangent to the TPR axis and indicating the hit rate with zero commission errors. In this case, the FNR corresponds to the complementary value of this TPRmax, which in turn corresponds to omission errors for $FPR = 0$. Thus, the shorter the length of the ROC curve touching the TPR axis, the higher the omission error.

In the third analysis, we observed a decrease in omission errors as the number of samples erroneously classified as water (FP) increased, from zero to 50 points classified as false positives. For this, we established thresholds considering the highest, the twentieth-highest, and the fiftieth-highest values of each index from points located in non-WSs. It is important to note that these numbers of samples were arbitrarily defined, and the behavior of FN errors was evaluated solely by changing the quantity of FP.

TABLE 3: The analyses were used for comparing spectral indices.

Analysis	Interpretation	Equation
The area under the partial ROC curve	The larger the area, the better the index performs in differentiating between WSs and Non-Water Surfaces.	$pAUC = \int_0^x TPR(fpr) d_{fpr} \quad (7)$
Threshold established by the highest value of the index in Non-Water Surfaces	The larger the length of the ROC curve tangent to the TPR axis and the lower the FNR value for zero false positives, the greater the WSs mapped.	$T > x_{0max}$ Where: x_0 is the highest index value in non-water surfaces.
Threshold established by the twentieth highest value of the index in WSs.	The smaller the FNR, the greater the WSs mapped, considering 20 points classified as FP.	$T > x'_{020} \text{ and } T > x'_{050}$ Where: x'_{020} is the twentieth index value in non-WSs. x'_{050} is the fiftieth index value in non-WSs.

III. RESULTS

As observed in Fig. 4 and Table 4, the RWI, MNDWI, NDWI, and $AWEI_{nsh}$ indices exhibited close values of the area under the pROC curve (Eq. 7), considering FPR values less than or equal to 0.02, for virtually all analyzed locations, ranging from 0.01568 to 0.01970, except for Curitiba, where NDWI had a value of 0.00115. The worst results were found with the $AWEI_{sh}$ index, which got values well below the other indices, ranging from 0.00053 to 0.01085. The Length of the pROC Curve tangent to the TPR axis corresponds to the proportion of hits considering the absence of FP. As observed, the pROC curve of $AWEI_{nsh}$ was very close to the TPR axis in Curitiba, Porto Alegre, and Buenos Aires but did not touch it, indicating the inability to correctly classify any water samples without considering the presence of commission errors (FP inclusion), considering the samples used. The pROC curve of $AWEI_{sh}$ was further away from the TPR axis.

Unlike the metric of the area under the pROC Curve, the values found for the Length of the pROC Curve tangent to the TPR axis were more dispersed, with larger amplitudes (ranging from 0 - 0.94961). It was expected that the variability of the results obtained with spectral indices would increase with a higher restriction of the error rate. It was also noted that the hits were higher for locations with more water samples collected in maritime, lake, and estuarine environments, as with Florianópolis, Porto Alegre, and Viña del Mar. The RWI obtained the best results in three out of the six locations, namely Curitiba, Buenos Aires, and Viña del Mar, besides the best overall result considering all the cities included in the analysis.

Finally, the last three columns of Table 4 show that the decrease in the miss rate is associated with an increase in FP errors. This behavior was observed in all analyzed indices except for the $AWEI_{sh}$, where no variations were found in any of the analyzed cities, resulting in the erroneous classification of all water samples. The best performances were found with the RWI, MNDWI, and NDWI indices, which showed lower miss rate values despite variations within each location and among locations. Our observations indicated that selecting a single index as the best for each area was not possible given the indices, period, and conditions considered. However, considering the six cities, the RWI achieved the best performance in three (Curitiba, Buenos Aires, and Viña del Mar) and all areas together.

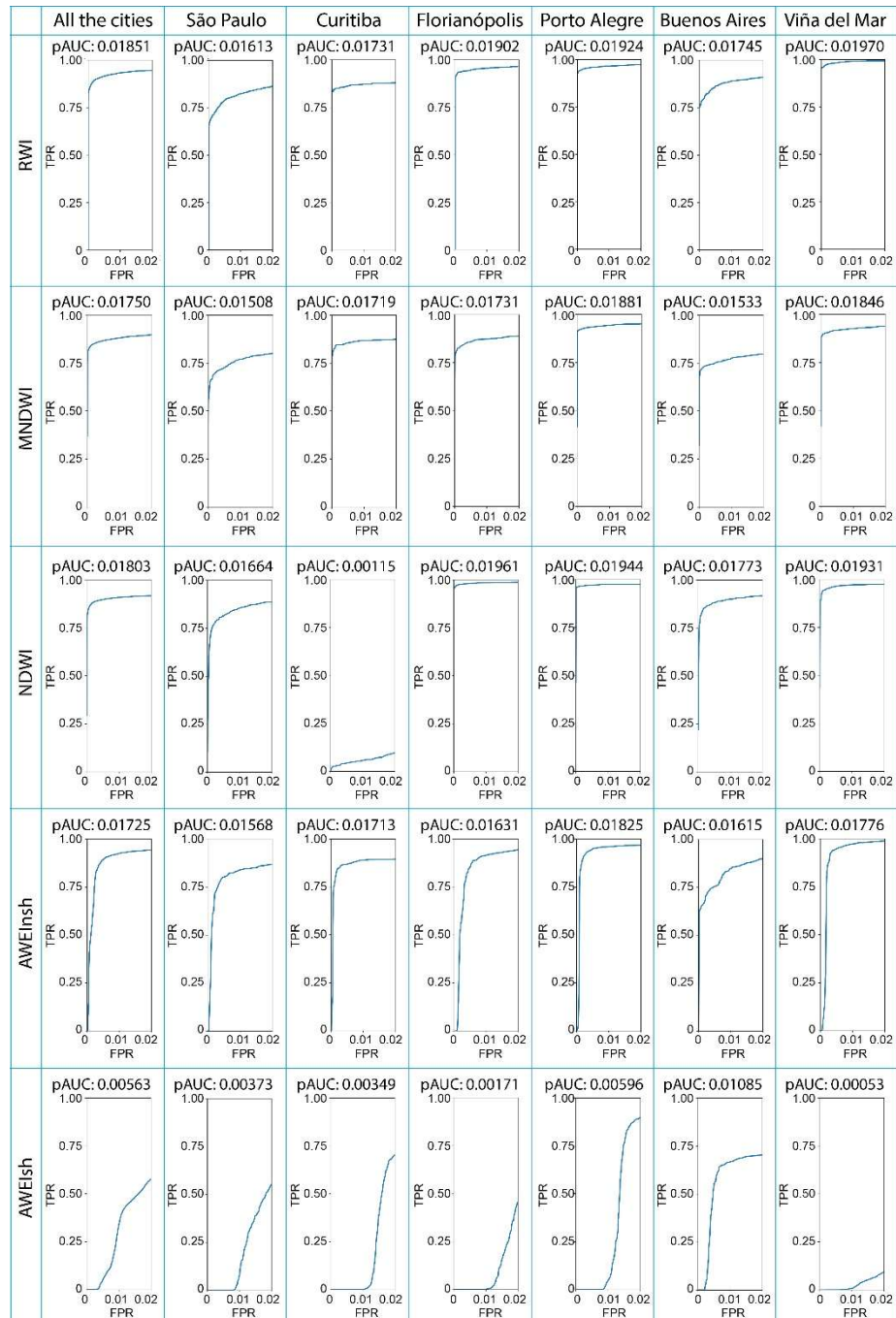


Fig. 4. Partial ROC curve up to 0.02 FPR indicating the cities with the best performances by index.

TABLE 4: Areas under the ROC curve and misclassification water points. Spectral indices with the best performances of each analysis are highlighted in bold.

Region	Water class	Index	Area under pROC Curve (FPR \leq 0,02)	Length of pROC Curve tangent to TPR axis (FPR = 0,00)	Miss rate (%)		
					Zero false positive points	20 false positive points	50 false positive points
					Limiar: $> x_{0_{max}}$	Limiar: $> x'_{0_{20}}$	Limiar: $> x'_{0_{50}}$
All the cities		RWI	0.01851	0.78394	21.61	15.48	14.07
		MNDWI	0.01750	0.75284	24.72	18.74	17.52
		NDWI	0.01803	0.55384	44.62	18.54	16.64
		AWEI _{nsh}	0.01725	0	100.00	99.70	85.25
		AWEI _{sh}	0.00563	0	100.00	100	100
São Paulo	polluted river, artificial ponds	RWI	0.01613	0.50716	49,28	30.92	23.05
		MNDWI	0.01508	0.55534	44.47	33.98	28.39
		NDWI	0.01664	0.24609	75.39	32.16	19.27
		AWEI _{nsh}	0.01568	0	100.00	78.26	22.01
		AWEI _{sh}	0.00373	0	100.00	100	100
Curitiba	clearwater river, artificial pond with algae	RWI	0.01731	0.83013	16.99	15.06	13.25
		MNDWI	0.01719	0.77564	22.44	15.60	13.89
		NDWI	0.00115	0	100.00	97.22	95.09
		AWEI _{nsh}	0.01713	0	100.00	19.44	12.18
		AWEI _{sh}	0.00349	0	100.00	100	100
Florianópolis	sea, artificial pond	RWI	0.01902	0.89839	10.94	6.37	4.55
		MNDWI	0.01731	0.78815	21.18	16.59	12.83
		NDWI	0.01961	0.94839	5.16	2.51	1.65
		AWEI _{nsh}	0.01631	0	100.00	48.56	8.72
		AWEI _{sh}	0.00171	0	100.00	100	99.98
Porto Alegre	river, artificial ponds, and water treatment plant	RWI	0.01924	0.92284	7.72	5.86	4.27
		MNDWI	0.01881	0.89799	10.20	7.93	6.65
		NDWI	0.01944	0.93418	6.58	3.68	2.94
		AWEI _{nsh}	0.01825	0	100.00	77.66	6.02
		AWEI _{sh}	0.00596	0	100.00	100	100
Buenos Aires	river mouth, artificial ponds	RWI	0.01745	0.75187	24.81	20.39	12.73
		MNDWI	0.01533	0.66061	33.94	27.27	24.31
		NDWI	0.01773	0.40499	59.50	16.68	11.05
		AWEI _{nsh}	0.01616	0	100.00	34.12	22.21
		AWEI _{sh}	0.01085	0	100.00	100	37.36
Viña del Mar	sea and reservoir	RWI	0.01970	0.94961	5.04	3.01	1.31
		MNDWI	0.01846	0.86126	13.87	9.58	7.96
		NDWI	0.01931	0.86540	13.46	5.58	3.14
		AWEI _{nsh}	0.01776	0	100.00	84.38	4.1
		AWEI _{sh}	0.00053	0	100.00	100	99.87

IV. DISCUSSION

This research highlighted the complexity of mapping water surfaces (WSs) in urban contexts, where shadows, buildings, and dark materials (such as asphalt) with spectral characteristics similar to water introduce considerable errors in the classification process. Confusions involving shadow and water are common in studies mapping urban areas using satellite images, and they were well-documented in the literature [29], [32], [33], [37], [45], [46], [47].

High specificity was prioritized because mistaking non-WSs as water is not desirable. pROC may be useful in practical applications, accepting a limited range of specificity or sensitivity [48] and enabling performance evaluation in a specific region of the ROC curve [49].

The results presented in this study demonstrated that the percentage of samples correctly classified over WSs varies from one index to another. In their study in the Poyang Lake Basin (southeast China), Zhou et al [50], highlighted that the performance of indices in mapping water bodies also varied according to the satellite images used when comparing different indices constructed with Landsat-7/8 and Sentinel-2 satellite images.

Observing the pROC (Fig. 4), it is noticeable that an index performs best at $FPR = 0$, but this may not hold true when commission errors are accepted. For the selected thresholds related to the number of false positives (Table 4), this occurred in São Paulo, Curitiba, and Buenos Aires. On the other hand, it is also possible for the index to perform best across multiple thresholds, as observed in Florianópolis and Porto Alegre for NDWI, and in Viña del Mar and across all cities for RWI.

In our study, the RWI, MNDWI, and NDWI indices achieved the best performances in the analyses of the pROC curves and miss rates, with their performances varying according to the locations. Although the $AWEI_{sh}$ index is considered efficient for delineating WSs in environments with shadow occurrence [30], [33], [51], here it was not efficient, presenting along with $AWEI_{nsh}$ the worst results in the overall analysis. Such results are compatible with studies by Li et al. [46], which report that such indices may not yield the expected results in areas with mountain and building shadows due to the noise generated by the shadow in classification, which leads to higher commission errors.

Fig. 5 shows a subarea of São Paulo, displaying water surfaces and commissions that would be mapped as water using thresholds corresponding to zero, 20, and 50 false-positive sample points. False alarms were observed in shadows for the RWI and NDWI indices, while commissions also occurred on bright rooftops for the MNDWI, a problem also noted by Chang et al. [51].



Fig. 5. Pixels classified as water, considering zero, 20, and 50 sample points as false alarms, are shown in yellow, orange, and red, respectively. Centroid coordinates -46.68683 W, -23.59242 S.

Mappings were produced (Fig. 6) to spatially understand the performance of the indices RWI, MNDWI, and NDWI concerning correct detections (length of the curve segment tangent to the TPR axis) and failures for $FPR=0$. The best index for some areas was inefficient in detecting one or more classes of water bodies. For instance, in Porto Alegre, NDWI did not detect an artificial lagoon, and in Buenos Aires, RWI and MNDWI did not detect water in a water treatment plant.


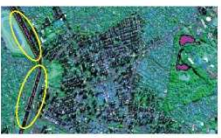

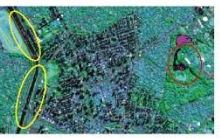
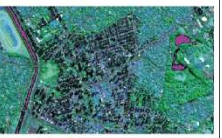
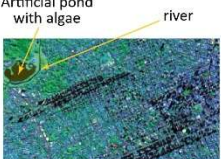
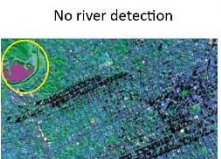
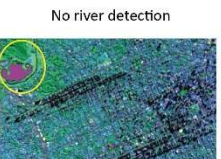
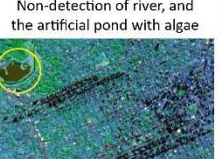
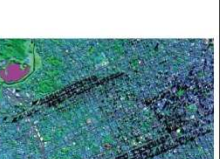
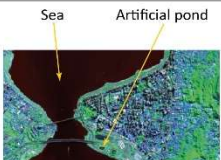
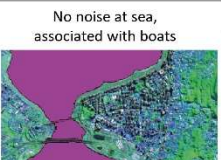
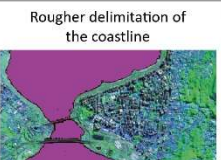
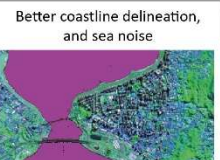

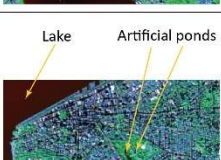
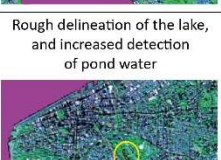
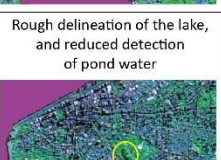
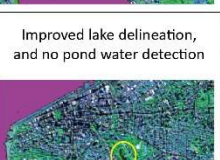

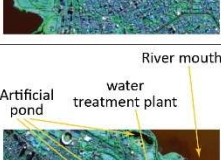
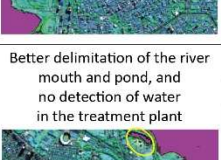
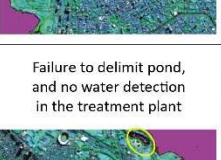
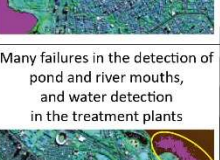

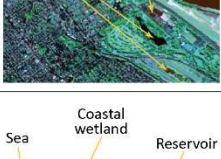


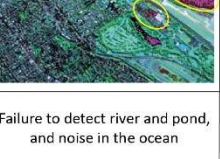

	False color composition, Green, Nir, and Swir1 bands	RWI	MNDWI	NDWI	Integrated indexes
São Paulo	 Polluted river Artificial ponds	 Failure to delimit polluted river	 Better delimit polluted river	 Failure to delimit polluted river and artificial ponds	
Curitiba	 Artificial pond with algae river	 No river detection	 No river detection	 Non-detection of river, and the artificial pond with algae	
Florianópolis	 Sea Artificial pond	 No noise at sea, associated with boats	 Rougher delineation of the coastline	 Better coastline delineation, and sea noise	
Porto Alegre	 Lake Artificial ponds	 Rough delineation of the lake, and increased detection of pond water	 Rough delineation of the lake, and reduced detection of pond water	 Improved lake delineation, and no pond water detection	
Buenos Aires	 River mouth Artificial pond water treatment plant	 Better delineation of the river mouth and pond, and no detection of water in the treatment plant	 Failure to delimit pond, and no water detection in the treatment plant	 Many failures in the detection of pond and river mouths, and water detection in the treatment plants	
Viña del Mar	 Sea Coastal wetland Reservoir	 Better delineation of pond, rivers, and sea	 No river detection, failure to delimit the pond and noise in the ocean	 Failure to detect river and pond, and noise in the ocean	

Fig. 6. Ws detection without commission errors. The water surfaces are indicated in magenta.

Considering the context in which the analyses were performed, the MNDWI had better results in polluted water environments. The NDWI, in turn, was better in marine and lake environments. The RWI achieved better results in maritime environments, river mouths (with suspended sediments), and lagoons with aquatic vegetation. Because the RWI was more adherent to the diversity of environments, in the overall result, considering all cities, its performance was also superior to the other indices. These results corroborate with the studies of Sun et al. [53] and Li et al. [54] that compared the performance of different water indices in China (Shaanxi and Upper Yellow River, respectively) with the aim of mapping water bodies and both studies highlighted the importance of considering the complementarity of the indices to improve mapping performance. Thus, according to Li et al. [54], while the MNDWI is better for mapping water bodies in urban areas, the $AWEI_{sh}$ is

better in areas with vegetation. Sun et al. [53] emphasized that the NDWI and MNDWI complement each other, and therefore, both should be used to extract different types of water features.

Following the reasoning of index complementarity, Fig. 7 shows the percentage of water points correctly classified considering the RWI, NDWI, and MNDWI indices. The Venn diagram shows the intersection, the union (all circles), and the differences of each set. The intersection of all sets (represented by gray color) indicates the proportion of samples correctly classified as water by all indices. The intersection of only two indices means the third index doesn't classify the water (represented by salmon, lilac, and light green colors). Finally, the difference of one set in relation to the others indicates the correct classification by only one of the indices (represented by subtractive primary colors - magenta, yellow, and cyan).

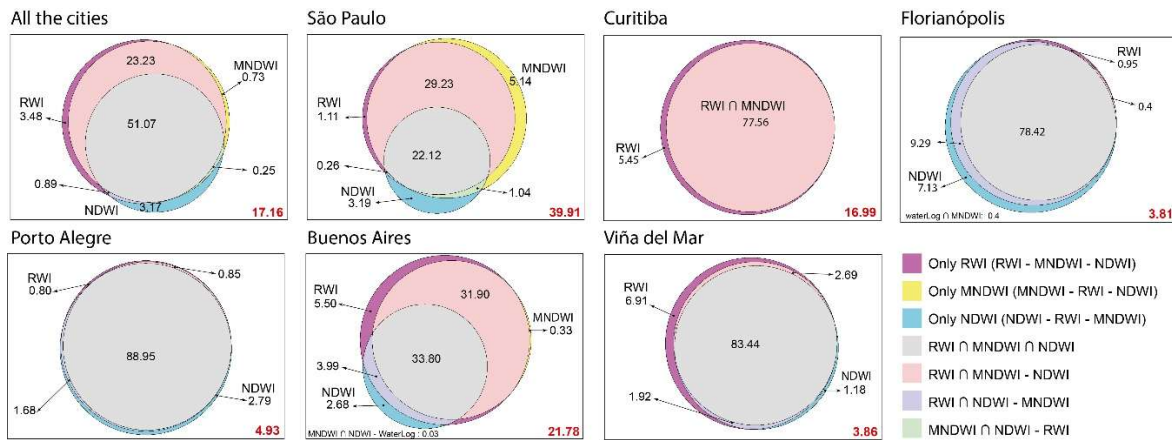


Fig. 7. Venn Diagram with the percentage of sample points classified as water for the RWI, MNDWI, and NDWI indices. The values highlighted in red in the graphs represent sample points incorrectly classified as water (False Negative Rate - FNR). The union of all sets equals 100 - FNR. Thus: All Cities = 82.84%; São Paulo = 60.09%; Curitiba = 83.01%; Florianópolis = 96.19%; Porto Alegre = 95.07%; Buenos Aires = 78.22%; Viña Del Mar = 96.14%.

As shown (Fig. 6 and Fig. 7), the combination of the three indices (RWI, NDWI, and MNDWI) would allow for the correct classification of a larger water area without commission errors. Regarding the sample points, the increase in TPR was achieved by considering the union of the sets of points correctly classified as water, for FPR = 0, from each of the indices (RWI, MNDWI, and NDWI).

Thus, the highest TPR were found in Florianópolis (96.19%), Viña del Mar (96.14%), and Porto Alegre (95.07%). Furthermore, the contribution of RWI was observed for all locations. In Niña del Mar, Buenos Aires, and Curitiba, the contribution of RWI is more significant, with an increase of 6.91%, 5.50%, and 5.45% in the mapping, respectively. In Florianópolis, the contribution of NDWI was more significant (7,13%). This result reinforces our finding that RWI performs better for coastal environments with or without sediments and lagoons with aquatic vegetation. In addition, MNDWI was a subset of RWI in Curitiba, Florianópolis, Porto Alegre, and Viña del Mar.

V. V. CONCLUSION

This study contributes to the field of water surface mapping by presenting elements that can aid in the development of more effective methodologies for monitoring water resources, public policies, and mitigating the effects of climate change. In some places, the proposed spectral index, RWI, has proven to be quite promising compared to other well-known indices in the literature. In the tests conducted (partial receiver operating characteristic curve (pROC) and miss rates), RWI achieved results that were compatible, yet different, from NDWI and MNDWI. In six analyzed locations (São

Paulo, Curitiba, Florianópolis, Porto Alegre, Buenos Aires, and Viña del Mar), RWI achieved better results in three and the best overall result. When analyzed using a Venn diagram, RWI was more effective in correctly classifying water points omitted by the other indices. Additionally, in four locations, the set of correctly classified points by MNDWI was a subset of those classified by RWI. We found that the proposed index's best contribution is in improving the mapping of water surfaces inside urban areas and the delimitation of the coastal and riverine lines.

VI. REFERENCES

- [1] I. A. Shiklomanov and J. C. Rodda, *World water resources at the beginning of the twenty-first century*. Cambridge University Press, 2003.
- [2] L. Wang-Erlandsson et al., “A planetary boundary for green water,” Jun. 01, 2022, Springer Nature. doi: 10.1038/s43017-022-00287-8.
- [3] H. Dolman, *Biogeochemical Cycles and Climate*. Oxford University Press, 2019.
- [4] M. L. Carroll, J. R. Townshend, C. M. DiMiceli, P. Noojipady, and R. A. Sohlberg, “A new global raster water mask at 250 m resolution,” *Int J Digit Earth*, vol. 2, no. 4, pp. 291–308, 2009, doi: 10.1080/17538940902951401.
- [5] F. Papa, C. Prigent, F. Aires, C. Jimenez, W. B. Rossow, and E. Matthews, “Interannual variability of surface water extent at the global scale, 1993-2004,” *Journal of Geophysical Research Atmospheres*, vol. 115, no. 12, 2010, doi: 10.1029/2009JD012674.
- [6] M. Rodell et al., “Emerging trends in global freshwater availability,” *Nature*, vol. 557, no. 7707, pp. 651–659, May 2018, doi: 10.1038/s41586-018-0123-1.
- [7] J. Dąbrowska et al., “Between flood and drought: How cities are facing water surplus and scarcity,” Nov. 01, 2023, Academic Press. doi: 10.1016/j.jenvman.2023.118557.
- [8] Md. J. Hossain, Md. M. Mahmud, and S. T. Islam, “Monitoring spatiotemporal changes of urban surface water based on satellite imagery and Google Earth Engine platform in Dhaka City from 1990 to 2021,” *Bull Natl Res Cent*, vol. 47, no. 1, Oct. 2023, doi: 10.1186/s42269-023-01127-5.
- [9] N. Akhtar, M. I. Syakir Ishak, S. A. Bhawani, and K. Umar, “Various natural and anthropogenic factors responsible for water quality degradation: A review,” Oct. 01, 2021, MDPI. doi: 10.3390/w13192660.
- [10] C. Li-An, L. Billa, and M. Azari, “Anthropocene climate and landscape change that increases flood disasters,” *International Journal of Hydrology*, vol. 2, no. 4, 2018, doi: 10.15406/ijh.2018.02.00115.
- [11] B. Manandhar, S. Cui, L. Wang, and S. Shrestha, “Urban Flood Hazard Assessment and Management Practices in South Asia: A Review,” Mar. 01, 2023, MDPI. doi: 10.3390/land12030627.
- [12] V. Rözer, S. Mehryar, and S. Surminski, “From managing risk to increasing resilience: a review on the development of urban flood resilience, its assessment and the implications for decision making,” *Environmental Research Letters*, vol. 17, no. 12, Dec. 2022, doi: 10.1088/1748-9326/aca8bc.
- [13] F. Laurien, J. G. C. Martin, and S. Mehryar, “Climate and disaster resilience measurement: Persistent gaps in multiple hazards, methods, and practicability,” Jan. 01, 2022, Elsevier B.V. doi: 10.1016/j.crm.2022.100443.

- [14] J. Juan Li, X. rong Wang, X. jun Wang, W. chun Ma, and H. Zhang, "Remote sensing evaluation of urban heat island and its spatial pattern of the Shanghai metropolitan area, China," *Ecological Complexity*, vol. 6, no. 4, pp. 413–420, Dec. 2009, doi: 10.1016/j.ecocom.2009.02.002.
- [15] Z. Cai, G. Han, and M. Chen, "Do water bodies play an important role in the relationship between urban form and land surface temperature?," *Sustain Cities Soc*, vol. 39, pp. 487–498, May 2018, doi: 10.1016/j.scs.2018.02.033.
- [16] E. A. Hathway and S. Sharples, "The interaction of rivers and urban form in mitigating the Urban Heat Island effect: A UK case study," *Build Environ*, vol. 58, pp. 14–22, Dec. 2012, doi: 10.1016/j.buildenv.2012.06.013.
- [17] N. E. Theeuwes, A. Solcerová, and G. J. Steeneveld, "Modeling the influence of open water surfaces on the summertime temperature and thermal comfort in the city," *Journal of Geophysical Research Atmospheres*, vol. 118, no. 16, pp. 8881–8896, Aug. 2013, doi: 10.1002/jgrd.50704.
- [18] Millennium Ecosystem Assessment (Program), *Ecosystems and human well-being : synthesis*. Island Press, 2005.
- [19] W. Zhang, H. Li, Q. Xiao, and X. Li, "Urban rivers are hotspots of riverine greenhouse gas (N₂O, CH₄, CO₂) emissions in the mixed-landscape chaohu lake basin," *Water Res*, vol. 189, Feb. 2021, doi: 10.1016/j.watres.2020.116624.
- [20] X. Y. Zhuge, X. Zou, and Y. Wang, "A Fast Cloud Detection Algorithm Applicable to Monitoring and Nowcasting of Daytime Cloud Systems," *IEEE Transactions on Geoscience and Remote Sensing*, vol. 55, no. 11, pp. 6111–6119, Nov. 2017, doi: 10.1109/TGRS.2017.2720664.
- [21] J. T. Jensen, *Remote Sensing of the Environment: An Earth Resource Perspective*, 2nd ed. Prentice Hall, 2000.
- [22] T. Soomets et al., "Comparison of lake opticalwater types derived from sentinel-2 and sentinel-3," *Remote Sens (Basel)*, vol. 11, no. 23, Dec. 2019, doi: 10.3390/rs11232883.
- [23] A. G. Dekker, T. J. Malthus, M. M. Wijnen, and E. Seyhan, "The Effect of Spectral Bandwidth and Positioning on the Spectral Signature Analysis of Inland Waters*," 1992.
- [24] E. Knaeps, A. I. Dogliotti, D. Raymaekers, K. Ruddick, and S. Sterckx, "In situ evidence of non-zero reflectance in the OLCI 1020nm band for a turbid estuary," *Remote Sens Environ*, vol. 120, pp. 133–144, May 2012, doi: 10.1016/j.rse.2011.07.025.
- [25] J. J. Wang, X. X. Lu, Y. Zhou, and S. C. Liew, "Suspended sediment concentrations estimate in highly turbid rivers: A field spectral survey," *Remote Sensing Letters*, vol. 4, no. 4, pp. 409–417, Apr. 2013, doi: 10.1080/2150704X.2012.743689.
- [26] P. S. Frazier and K. J. Page, "Water Body Detection and Delineation with Landsat TM Data," *Photogramm Eng Remote Sensing*, vol. 66, no. 12, pp. 1461–1467, 2000, Accessed: Jan. 02, 2023. [Online]. Available: https://web.pdx.edu/~nauna/resources/5-2000_dec_1461-1467.pdf
- [27] C. Jiao, S. Wang, S. Song, and B. Fu, "Long-term and seasonal variation of open-surface water bodies in the Yellow River Basin during 1990–2020," *Hydrol Process*, vol. 37, no. 3, Mar. 2023, doi: 10.1002/hyp.14846.
- [28] M. H. R. Moghaddam, A. Sedighi, and M. A. Fayyazi, "Applying MNDWI index and linear directional mean analysis for morphological changes in the Zarriné-Rūd River," *Arabian Journal of Geosciences*, vol. 8, no. 10, pp. 8419–8428, Oct. 2015, doi: 10.1007/s12517-015-1795-6.

- [29] X. Wang et al., “A robust Multi-Band Water Index (MBWI) for automated extraction of surface water from Landsat 8 OLI imagery,” *International Journal of Applied Earth Observation and Geoinformation*, vol. 68, pp. 73–91, Jun. 2018, doi: 10.1016/j.jag.2018.01.018.
- [30] G. L. Feyisa, H. Meilby, R. Fensholt, and S. R. Proud, “Automated Water Extraction Index: A new technique for surface water mapping using Landsat imagery,” *Remote Sens Environ*, vol. 140, pp. 23–35, Jan. 2014, doi: 10.1016/j.rse.2013.08.029.
- [31] E. F. Justiniano et al., “Proposal for an index of roads and structures for the mapping of non-vegetated urban surfaces using OSM and Sentinel-2 data,” *International Journal of Applied Earth Observation and Geoinformation*, vol. 109, no. April, p. 102791, May 2022, doi: 10.1016/j.jag.2022.102791.
- [32] X. Yang, Q. Qin, P. Grussenmeyer, and M. Koehl, “Urban surface water body detection with suppressed built-up noise based on water indices from Sentinel-2 MSI imagery,” *Remote Sens Environ*, vol. 219, no. September 2017, pp. 259–270, 2018, doi: 10.1016/j.rse.2018.09.016.
- [33] Y. Li, X. Gong, Z. Guo, K. Xu, D. Hu, and H. Zhou, “An index and approach for water extraction using Landsat–OLI data,” *Int J Remote Sens*, vol. 37, no. 16, pp. 3611–3635, Aug. 2016, doi: 10.1080/01431161.2016.1201228.
- [34] S. K. McFeeters, “The use of the Normalized Difference Water Index (NDWI) in the delineation of open water features,” *Int J Remote Sens*, vol. 17, no. 7, pp. 1425–1432, 1996, doi: 10.1080/01431169608948714.
- [35] H. Xu, “Modification of normalised difference water index (NDWI) to enhance open water features in remotely sensed imagery,” *Int J Remote Sens*, vol. 27, no. 14, pp. 3025–3033, Jul. 2006, doi: 10.1080/01431160600589179.
- [36] O. E. Malahlela, “Inland waterbody mapping: towards improving discrimination and extraction of inland surface water features,” *Int J Remote Sens*, vol. 37, no. 19, pp. 4574–4589, Oct. 2016, doi: 10.1080/01431161.2016.1217441.
- [37] Z. Wang, J. Liu, J. Li, and D. D. Zhang, “Multi-Spectral Water Index (MuWI): A Native 10-m Multi-Spectral Water Index for accurate water mapping on sentinel-2,” *Remote Sens (Basel)*, vol. 10, no. 10, Oct. 2018, doi: 10.3390/rs10101643.
- [38] J. Li, B. Peng, Y. Wei, and H. Ye, “Accurate extraction of surface water in complex environment based on Google Earth Engine and Sentinel-2,” *PLoS One*, vol. 16, no. 6 June, Jun. 2021, doi: 10.1371/journal.pone.0253209.
- [39] Z. Jiang, J. Qi, S. Su, Z. Zhang, and J. Wu, “Water body delineation using index composition and HIS transformation,” *Int J Remote Sens*, vol. 33, no. 11, pp. 3402–3421, 2012, doi: 10.1080/01431161.2011.614967.
- [40] W. Bie, T. Fei, X. Liu, H. Liu, and G. Wu, “Small water bodies mapped from Sentinel-2 MSI (MultiSpectral Imager) imagery with higher accuracy,” *Int J Remote Sens*, vol. 41, no. 20, pp. 7912–7930, Oct. 2020, doi: 10.1080/01431161.2020.1766150.
- [41] J. W. Rouse, R. H. Hass, J. A. Schell, and D. W. Deering, “Monitoring vegetation systems in the great plains with ERTS,” *Third Earth Resources Technology Satellite (ERTS) symposium*, vol. 1, pp. 309–317, 1973, doi: citeulike-article-id:12009708.
- [42] Y. Zha, J. Gao, and S. Ni, “Use of normalized difference built-up index in automatically mapping urban areas from TM imagery,” *Int J Remote Sens*, vol. 24, no. 3, pp. 583–594, Feb. 2003, doi: 10.1080/01431160304987.

- [43] E. Knaeps et al., “The SeaSWIR dataset,” *Earth Syst Sci Data*, vol. 10, no. 3, pp. 1439–1449, Aug. 2018, doi: 10.5194/essd-10-1439-2018.
- [44] K. Uudeberg, I. Ansko, G. Põru, A. Ansper, and A. Reinart, “Using optical water types to monitor changes in optically complex inland and coastal waters,” *Remote Sens (Basel)*, vol. 11, no. 19, Oct. 2019, doi: 10.3390/rs11192297.
- [45] Q. Guo, R. Pu, J. Li, and J. Cheng, “A weighted normalized difference water index for water extraction using landsat imagery,” *Int J Remote Sens*, vol. 38, no. 19, pp. 5430–5445, Oct. 2017, doi: 10.1080/01431161.2017.1341667.
- [46] L. Li, H. Su, Q. Du, and T. Wu, “A novel surface water index using local background information for long term and large-scale Landsat images,” *ISPRS Journal of Photogrammetry and Remote Sensing*, vol. 172, pp. 59–78, Feb. 2021, doi: 10.1016/j.isprsjprs.2020.12.003.
- [47] Z. Wen, C. Zhang, G. Shao, S. Wu, and P. M. Atkinson, “Ensembles of multiple spectral water indices for improving surface water classification,” *International Journal of Applied Earth Observation and Geoinformation*, vol. 96, Apr. 2021, doi: 10.1016/j.jag.2020.102278.
- [48] H. Ma, A. I. Bandos, and D. Gur, “On the use of partial area under the ROC curve for comparison of two diagnostic tests,” *Biometrical Journal*, vol. 57, no. 2, pp. 304–320, Mar. 2015, doi: 10.1002/bimj.201400023.
- [49] F. S. Nahm, “Receiver operating characteristic curve: overview and practical use for clinicians,” *Korean J Anesthesiol*, vol. 75, no. 1, pp. 25–36, Feb. 2022, doi: 10.4097/kja.21209.
- [50] Y. Zhou et al., “Open surface water mapping algorithms: A comparison of water-related spectral indices and sensors,” *Water (Switzerland)*, vol. 9, no. 4, Apr. 2017, doi: 10.3390/w9040256.
- [51] L. Chang, L. Cheng, C. Huang, S. Qin, C. Fu, e S. Li, “Extracting Urban Water Bodies from Landsat Imagery Based on mNDWI and HSV Transformation”, *Remote Sens (Basel)*, vol. 14, no 22, nov. 2022, doi: 10.3390/rs14225785.
- [52] A. Fisher, N. Flood, and T. Danaher, “Comparing Landsat water index methods for automated water classification in eastern Australia,” *Remote Sens Environ*, vol. 175, pp. 167–182, Mar. 2016, doi: 10.1016/j.rse.2015.12.055.
- [53] F. Sun, W. Sun, J. Chen, and P. Gong, “Comparison and improvement of methods for identifying waterbodies in remotely sensed imagery,” *Int J Remote Sens*, vol. 33, no. 21, pp. 6854–6875, 2012, doi: 10.1080/01431161.2012.692829.
- [54] D. Li et al., “Open-surface river extraction based on sentinel-2 MSI imagery and DEM Data: Case study of the upper yellow river,” *Remote Sens (Basel)*, vol. 12, no. 17, Sep. 2020, doi: 10.3390/RS12172737.